

# Electroweak Nucleon Structure with Parity Violating Electron Scattering

**R. González-Jiménez<sup>1</sup>, J. A. Caballero<sup>1</sup>, T. W. Donnelly<sup>2</sup>**

<sup>1</sup>Departamento de Física Atómica, Molecular y Nuclear, Universidad de Sevilla, Aptdo 1065, E-41080 Sevilla, Spain

<sup>2</sup>Center for Theoretical Physics, Laboratory for Nuclear Science and Department of Physics, Massachusetts Institute of Technology, Cambridge, Massachusetts 02139, USA

**Abstract.** The existence of the quark-antiquark sea in the nucleon, and in particular, the role played by the heavier strange pairs, has been firmly established. However, how the nucleon strangeness enters in the electromagnetic nucleon properties remains as an open question. Parity violation in elastic electron-nucleon scattering is studied with the basic goal of improving the understanding of electroweak hadronic structure with special emphasis on the strangeness content in the nucleon. Results for the parity-violating (PV) asymmetry are provided and compared with a large variety of data measured at very different kinematics.

## 1 Introduction

Over the years electron scattering has provided the most precise information on hadron and nuclear structure. Most of these studies have considered only the purely electromagnetic (EM) interaction, that is, parity-conserving (PC) electron scattering processes. The analysis of inclusive and semi-inclusive reactions, as well as the measurement of polarization observables in very different kinematical regimes, has allowed us to deepen very significantly our knowledge of the inner structure of hadrons and nuclei [1–5].

The weak interaction, although orders of magnitude weaker than the EM one, also plays a role in electron scattering processes. The interest in parity-violating (PV) observables through the description of electron scattering, denoted simply as PV electron scattering to contrast it with PC scattering where only the EM interaction enters, has had three basic motivations: i) to serve in testing the Standard Model of electroweak interactions, ii) to provide a tool for determining the electroweak form factors of the nucleon, and iii) to employ the semi-leptonic electroweak interaction as a probe of nucleon structure. In this work, our interest is restricted to the second point. It is important to point out that the smallness of the weak coupling, compared with the EM one, forces one to analyze observables strictly linked to parity-violating effects, requiring at the same time,

excellent control of the EM ingredients entering the description of the scattering reaction. Furthermore, from the combined study of electron scattering from the proton and from nuclei, involving elastic, inelastic and quasielastic regimes, useful constraints on the form factors should emerge. In this work we restrict ourselves to elastic PV electron-proton scattering.

The existence of the quark sea and its influence on some basic properties of the nucleon (mass, spin, magnetic moment) has been firmly established in several experimental studies [6–12]. However, the specific role of  $s\bar{s}$  pairs in the static EM properties of the nucleon still remains elusive. In this work our interest is focused on the contribution of the strange quarks connected to the electroweak current of the nucleon.

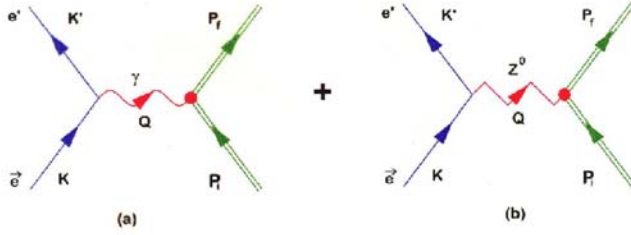


Figure 1. One-boson-exchange diagrams for electron-proton scattering: (a) EM interaction and (b) WNC interaction.

A complete description of the scattering process between electrons and hadrons and/or nuclei requires not only the dominant EM interaction but also the residual weak interaction, the latter being responsible for parity violation. Assuming the Born Approximation (BA), *i.e.*, only one virtual boson exchanged in the process (photon  $\gamma$  for the EM interaction and neutral  $Z$  boson for the weak process), the corresponding Feynman diagrams are depicted in Figure 1. Because of the smallness of the weak coupling constant compared with the EM one, the leading order PV contribution arises from the interference between the two processes shown diagrammatically in Figure 1. The contribution of the purely weak term  $|\mathcal{M}_Z|^2$  is typically negligible. It is important to stress that the PV interference contribution,  $Re(\mathcal{M}_\gamma^* \mathcal{M}_Z)$  is about  $\sim 4$ – $5$  orders of magnitude smaller than the purely EM one,  $|\mathcal{M}_\gamma|^2$ . Hence, the determination of parity violation through electron scattering requires very precise measurements of observables that only exist if the weak interaction comes into play.

Parity violation in electron scattering emerges from the measurement of the helicity asymmetry, also denoted as PV asymmetry, that is given as the ratio between the difference and the sum of the cross sections corresponding to right and left-handed incident polarized electrons,

$$\mathcal{A}^{PV} = \frac{d\sigma^+ - d\sigma^-}{d\sigma^+ + d\sigma^-} = \frac{d\sigma^{PV}}{d\sigma^{PC}}, \quad (1)$$

where the index  $\pm$  indicates the helicity of the incident electron beam. It is important to point out that the above cross sections refer to single-arm (inclusive) scattering of longitudinally polarized electrons with no hadronic/nuclear polarizations. Otherwise, parity-conserving effects that are generally much larger than the effects coming solely from PV, may also contribute to the asymmetry.

The purely EM cross section does not depend on the electron helicity, thus the difference in the numerator in Eq. (1) only enters because of the weak interaction, and therefore, a value of  $\mathcal{A}^{PV} \neq 0$  is a clear signature of PV effects (exchange of the  $Z$ -boson).

In this work we compare our theoretical predictions evaluated with several recent descriptions of the hadronic structure with all available  $\vec{e}p$  data. Electroweak radiative corrections as well as effects from higher-order terms in the description of the EM interaction have been incorporated in the analysis. The electroweak nucleon form factors that enter in the general expressions for the EM and WNC operators are analyzed in detail. Various kinematical regimes are considered and we analyze the sensitivity of  $\mathcal{A}^{PV}$  to the specific choices made for the nucleon's EM form factors. The influence of the  $s\bar{s}$  sea quark is also investigated in detail. Finally, we summarize our basic results and present our conclusions.

## 2 General Formalism for PV Elastic ( $\vec{e}, N$ ) Scattering

The processes we consider are represented in Figure 1. Here, an electron with four-momentum  $K^\mu = (\epsilon, \mathbf{k})$  and helicity  $h$  is scattered through an angle  $\theta_e$  to four-momentum  $K'^\mu = (\epsilon', \mathbf{k}')$ , exchanging a photon (EM interaction) or a neutral boson  $Z$  (weak interaction). The hadronic variables are  $P_i^\mu = (E_i, \mathbf{p}_i)$  the incident nucleon four-momentum and  $P_f^\mu = (E_f, \mathbf{p}_f)$  the final one. The transferred four-momentum in the process is given by  $Q^\mu = (K - K')^\mu = (P_f - P_i)^\mu = (\omega, \mathbf{q})$ . We use the convention and metric of [13] and accordingly, using the notation employed in previous work,  $Q^2 = \omega^2 - q^2 \leq 0$ .

Given the restriction to the Born Approximation, the helicity dependent ( $h$ ) differential cross section for the scattering process can be written as

$$\frac{d\sigma^{(h)}}{d\Omega_f} = \sigma_M \left( \frac{\epsilon_f}{\epsilon_i} \right) \left[ v_L R^L + v_T R^T - \frac{\mathcal{A}_0}{2} ((a_V - ha_A)(v_L \tilde{R}^L + v_T \tilde{R}^T) + (ha_V - a_A)v_T \tilde{R}^{T'}) \right], \quad (2)$$

where  $\sigma_M$  is the Mott cross section and  $\mathcal{A}_0$  is the scale of parity-violating effects [14–16]. The factors  $v_K$  are the lepton kinematical coefficients and  $R^K$  ( $\tilde{R}^K$ ) are the hadronic EM (weak) responses [4,5]. The labels  $K = L, T, T'$  indicate contributions along  $\mathbf{q}$  and transverse to  $\mathbf{q}$ , respectively.

Finally, after some algebra [16], the PV asymmetry can be written as

$$\mathcal{A}^{PV} = \mathcal{A}_E + \mathcal{A}_M + \mathcal{A}_A \quad (3)$$

with

$$\mathcal{A}_E = \frac{\mathcal{A}_0 a_A \varepsilon G_E^p \tilde{G}_E^p}{2 F^2}, \quad \mathcal{A}_M = \frac{\mathcal{A}_0 a_A \tau G_M^p \tilde{G}_M^p}{2 F^2}, \quad (4)$$

$$\mathcal{A}_A = -\frac{\mathcal{A}_0 a_V \sqrt{1 - \varepsilon^2} \sqrt{\tau(1 + \tau)} G_M^p \tilde{G}_A^p}{2 F^2}. \quad (5)$$

We have introduced  $\tau \equiv |Q^2|/4M^2$ ,  $\varepsilon = [1 + 2(1 + \tau) \tan^2 \theta_e/2]^{-1}$  and have assumed the vector and axial-vector electron couplings at tree level [14, 15], i.e.,  $a_V = -1 + 4 \sin^2 \theta_W$  and  $a_A = -1$ . The EM form factors of the proton,  $G_{E,M}^p$ , and the WNC ones,  $\tilde{G}_{E,M,A}^p$ , have been also considered. Finally, we define  $F^2 \equiv \varepsilon(G_E^p)^2 + \tau(G_M^p)^2$ .

The analysis of the PV asymmetry in different kinematical regions has been simplified by isolating the contributions linked to the electric, magnetic and axial-vector distributions.

### 3 Hadronic Structure

#### 3.1 Electroweak Structure of the Nucleon: $G_{E,M,A}^p$

In the Standard Model, including higher order corrections, the WNC form factors are given in terms of the EM ones ( $G_{E,M}^{p,n}$ ), the electroweak coupling constants (involving  $\sin^2 \theta_W$ ), the radiative corrections ( $R_V$ ) and the strange form factors ( $G_{E,M}^{(s)}$ ):

$$\tilde{G}_{E,M}^p = -a_V(1 + R_V^p)G_{E,M}^p - (1 + R_V^n)G_{E,M}^n - (1 + R_V^{(0)})G_{E,M}^{(s)}. \quad (6)$$

Likewise, the WNC axial-vector form factors can be decomposed into isovector ( $G_A^{(3)}$ ) and isoscalar ( $G_A^{(8)}$ ) contributions that can be determined from Gamow-Teller  $\beta$ -decay rates and hyperon  $\beta$ -decay measurements, respectively. Radiative corrections and coupling constants have been incorporated too. An additional strange axial-vector form factor also emerges (from  $s\bar{s}$  pair) and its value has been extracted from the analysis of  $\nu p/\bar{\nu} p$  experiments [16]:

$$\tilde{G}_A^p = \left( -2(1 + R_A^{T=1})G_A^{(3)} + \sqrt{3}R_A^{T=0}G_A^{(8)} + (1 + R_A^{(0)})G_A^{(s)} \right) G_D^A. \quad (7)$$

It is important to point out that the WNC proton form factors depend on both the proton and neutron EM form factors.

To conclude, we assume the radiative corrections to be constant [17] and the  $Q^2$ -dependence of the strange and axial-vector form factors is described by using a dipole function:

$$G_E^{(s)}(Q^2) = \rho_s \tau (1 + |Q^2|/M_V^2)^{-2}, \quad G_M^{(s)}(Q^2) = \mu_s (1 + |Q^2|/M_V^2)^{-2}, \quad (8)$$

$$G_D^A(Q^2) = (1 + |Q^2|/M_A^2)^{-2}. \quad (9)$$

In the above expressions,  $M_A$  is the axial mass parameter and  $\mu_s$  ( $\rho_s$ ) define the strangeness content in the magnetic (electric) channels. The vector mass is fixed to  $M_V = 0.84$  GeV.

### 3.2 Electromagnetic Structure of the Nucleon: $G_{E,M}^{p,n}$

As known, in the case of free (on-shell) nucleons and the purely EM interaction, the hadron structure is fully characterized by two functions: the electric ( $G_E^N$ ) and magnetic ( $G_M^N$ ) nucleon form factors.

In Figure 2 we present the EM nucleon form factors against  $|Q^2|$  for different models and compare them with data. The results have been normalized by the usual dipole function,  $G_D = (1 + \lambda_D^V \tau)^{-2}$  with  $\lambda_D^V = 4.97$ . These models are: Arrington and Sick (A-S) [18], Kelly [19], GKex [20–22] and Beluskin, Hammer and Meißner (BHM-qQCD and BHM-SC) [23]. As shown, all prescriptions provide reasonable descriptions of data at low  $|Q^2|$ , with a relatively

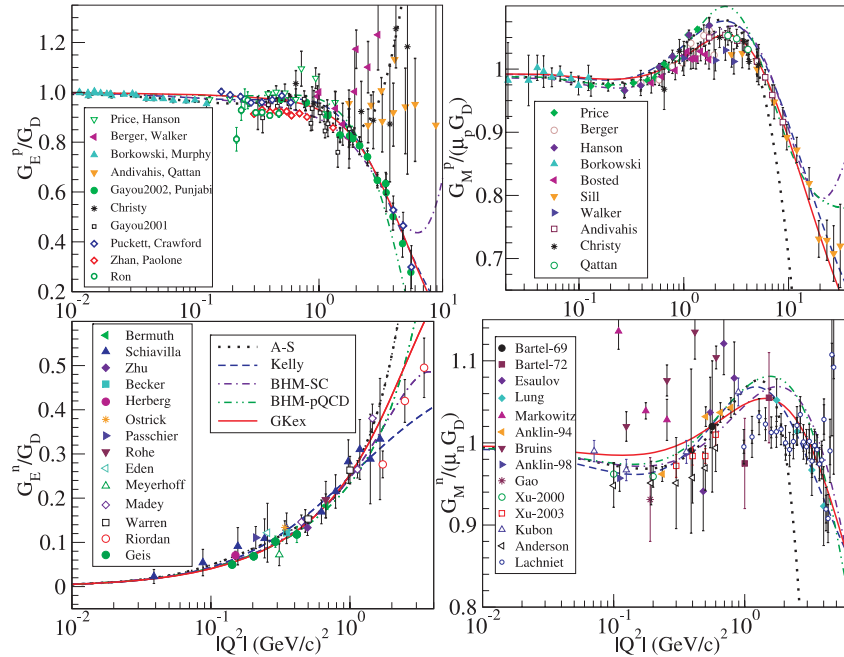


Figure 2. EM nucleon form factors obtained with different descriptions compared with data. The proton electric form factor (top-left panel) corresponding to Gayou2002, Gayou2001, Punjabi, Puckett, Zhan, Ron, Paolone and Crawford have been obtained from  $R_p$  data by dividing by the GKex model values of  $G_M^p / \mu_p$ . The same applies to Geis in the case of the electric neutron form factor (left-bottom), but using the GKex model  $G_M^n / \mu_n$ . See Ref. [24] for a complete list of references concerning data, that we omit here for loss of space.

small dispersion between the different curves. On the contrary, for increasing values of the transferred momentum the differences between the models go up significantly. It is important to point out the discrepancy in the top-left panel between data from Rosenbluth separation (Andivahis, Qattan, Christy) and polarization measurements (Gayou2002, Punjabi, Puckett, Crawford) at high  $|Q^2|$ .

## 4 Results

The various ingredients entering the description of the process, *i.e.*, the EM and WNC structure of the proton, and their effects on  $\mathcal{A}^{PV}$  are analyzed. We compare the results obtained with all data available that span a range in  $|Q^2|$  up to 1 (GeV/c)<sup>2</sup>.

### 4.1 Dependence with the EM Nucleon Structure

In Figure 3 we study the sensitivity shown by the PV asymmetry to the EM nucleon form factors. Only results based on the AS model clearly depart from the others for  $|Q^2|$ -values above 1.5 (GeV/c)<sup>2</sup>. For  $|Q^2|$  above 2 (GeV/c)<sup>2</sup> this discrepancy gets much larger, *i.e.*, consistent with the behavior shown by  $G_{E,M}^{p,n}$  in Figure 2.

Concerning the four remaining prescriptions: Kelly, GKex, BHM-SC and BHM-pQCD, they provide very close results for all transferred momentum values. The discrepancy is at most of the order of  $\sim 3\text{--}4\%$  at the limit  $|Q^2| = 2$  (GeV/c)<sup>2</sup> and is very similar for all scattering angles. At  $|Q^2| = 1$  (GeV/c)<sup>2</sup> (limit in the experimental data for the asymmetry) the dispersion between the four prescriptions is about  $\sim 3\%$  in the very forward case ( $\theta_e = 5^\circ$ ), and gets much smaller,  $\sim 0.7\%$ , for larger angles ( $\theta_e = 170^\circ$ ).

In order to get insight into the sensitivity of  $\mathcal{A}^{PV}$  with the EM nucleon structure at forward and backward scattering reactions, we isolate the contribution

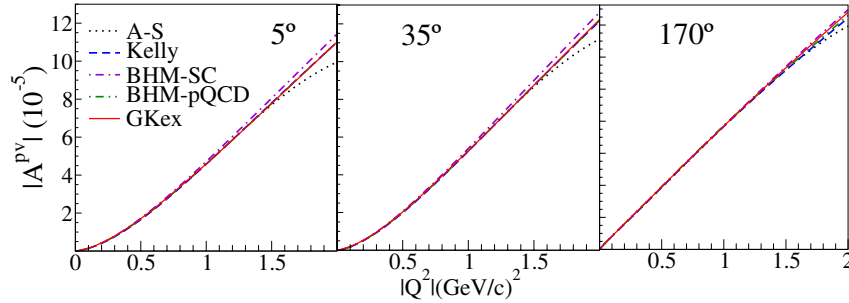


Figure 3. Absolute value of the PV asymmetry as a function of  $|Q^2|$ . Results are presented for six scattering angles and the five prescriptions considered in the previous section for the EM nucleon form factors. Radiative corrections have been included, but neglecting nucleon strangeness.

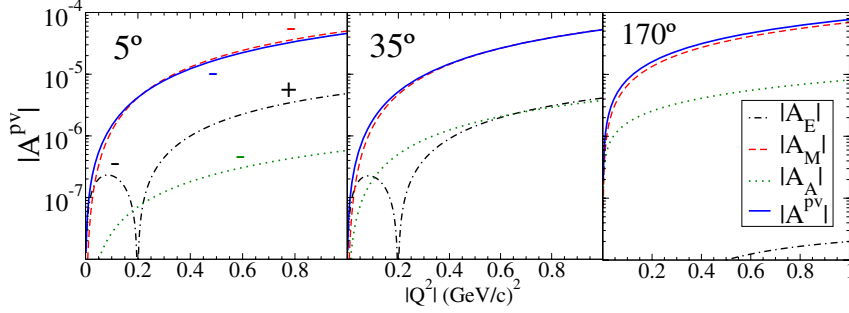


Figure 4. Separate contribution in the PV asymmetry coming from the electric (black dashed-dotted line), magnetic (red dashed line) and axial-vector (green dotted line) distributions (see Eq. (3)). The symbol  $+$  ( $-$ ) indicates the positive (negative) character of the corresponding response in the  $|Q^2|$  region selected. The full asymmetry (blue solid line) is also shown for reference. Results correspond to the GKex prescription. As in the previous figure, radiative corrections are included, but without strangeness in the nucleon.

given by the electric, magnetic and axial-vector distributions. This is shown in Figure 4. Note the absolute dominance of the magnetic contribution  $\mathcal{A}_M$  in all the kinematical situations. Concerning the electric and axial-vector terms, typically orders of magnitude smaller than  $\mathcal{A}_M$ , the relative predominance of one over the other depends on the specific kinematics. These results can be easily explained from the general expressions given in Eqs. (4,5). In the limit of very forward-angle scattering,  $\theta_e \rightarrow 0^\circ$ , we have  $\varepsilon \rightarrow 1$ . Thus, the axial-vector contribution  $\mathcal{A}_A$  approaches zero. In the backward-angle limiting case, *i.e.*,  $\theta_e \rightarrow 180^\circ$ , the factor  $\varepsilon \rightarrow 0$ . Hence, the electric term  $\mathcal{A}_E$  does not enter. Therefore, the PV asymmetry for backward-angle kinematics is entirely determined by the magnetic and axial-vector distributions.

## 4.2 Nucleon Strangeness

In Figure 5 we present the asymmetry for two backward angles. The three colors represent the asymmetry for three values of  $\mu_s$ . Each color band shows the uncertainty associated to the axial contribution, *i.e.*, the extreme lines of each color band have been computed by using  $M_A = 1.032$  and  $M_A = 1.35$  GeV. The slopes of the theoretical calculation are smaller than the behavior shown by data and it is difficult to describe both data setting the  $\mu_s$  parameter. However, the data error bands allow one to conclude that  $\mu_s = 0$  seems to be the case where theory and data agree better. As discussed previously, backward-angle measurement of  $\mathcal{A}^{PV}$  should be considered as a means to isolate the contribution of  $G_M^{(s)}$ . Results in Figure 5 show the significant sensitivity of the asymmetry to variations of the magnetic strangeness, in fact, much more important than effects introduced by other ingredients.

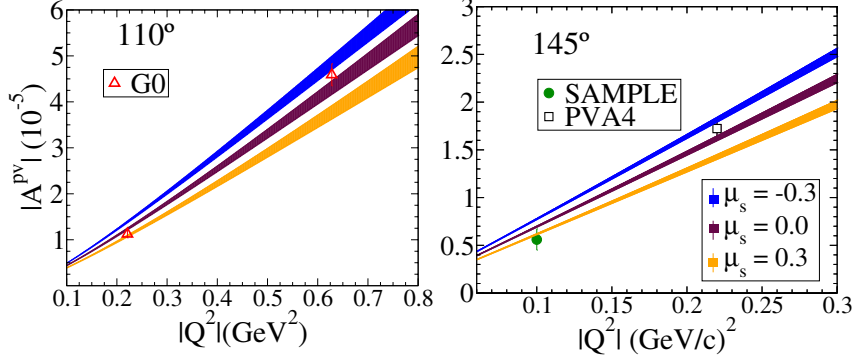


Figure 5. PV asymmetry for backward scattering angles:  $\theta_e = 110^\circ$  (left panels) and  $145^\circ$  (right panels). The GKex prescription for the EM form factors has been used. The width of the various curves incorporates the total uncertainty linked to the WNC axial-vector form factor description. In the left panel model is compared with data from G0 [25] experiment, in the right one, with data from SAMPLE [26] and PVA4 [27] experiments.

The analysis of forward-angle scattering kinematics is presented in Figure 6. In order to make the discussion that follows easier, the data have been separated in two basic categories: i) very forward-angle scattering, *i.e.*,  $\theta_e < 13^\circ$  (panel on the left) and ii) larger scattering angles,  $\theta_e \sim 35^\circ$  (right panel). In both cases theoretical results are compared with data taken at different kinematics. The width of the curves takes into account the uncertainty introduced by the description of the axial-vector form factor as discussed previously. Notice that the relative contribution of the WNC axial-vector form factor tends to cancel as  $\theta_e$  approaches zero and vice versa (see Figure 4).

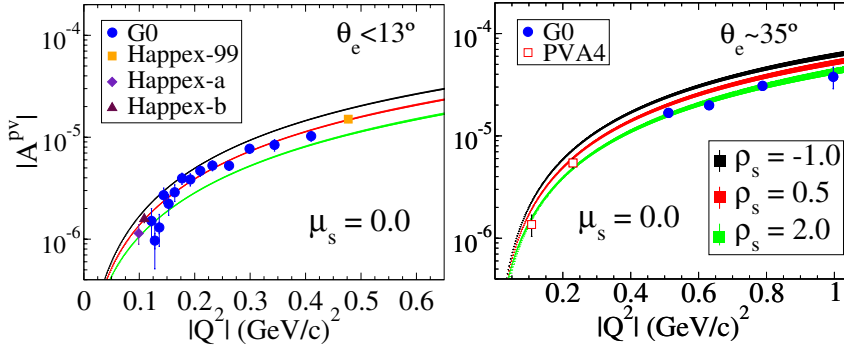


Figure 6. PV asymmetry evaluated at forward scattering angles compared with experimental data. The GKex prescription for the EM nucleon form factors has been used. The value of the static magnetic strange parameter is fixed to  $\mu_s = 0.0$  and results are presented for three values of the electric strange content given through  $\rho_s$ . The data are taken from [28–33]

The dependence of the PV asymmetry with the electric strangeness content  $\rho_s$  is clearly observable in all cases. The clear separation between the different curves for increasing  $|Q^2|$  may help us in disentangling which specific choice of electric strangeness is best suited to describe the data. This analysis should be coherent with the study applied to backward-angle kinematics where the focus is on the magnetic strange content. However, as already discussed in that situation, the analysis of data at forward-angle scattering and its comparison with theory introduces also some ambiguities that need to be clarified. As shown, given a specific  $\mu_s$ , the electric strangeness that provides the best accordance with data at  $\theta_e < 13^\circ$  overestimates, on the contrary, the behavior of data at larger  $\theta_e \sim 35^\circ$ .

## 5 Conclusion

The basic goal of the present study is to deepen our knowledge on the hadronic structure with a special focus on the analysis of strangeness content in the electroweak nucleon form factors. To do this, we have studied parity-violation electron-proton scattering. In recent years a great effort from the experimental and theoretical points of view has been devoted to this problem. New experiments have been devised and performed for a large variety of kinematical situations. Data reported at backward and forward scattering angles are compared in this work with theoretical calculations showing the role played by the different ingredients entering the description of the reaction mechanism.

Summarizing, the general discussion presented in previous sections clearly indicates that further studies and investigations are needed before definite conclusions on the strangeness content in the nucleon can be drawn. Not only the specific values of the strangeness content given through the parameters  $\mu_s$  and  $\rho_s$  should be reviewed, but also the specific functional dependence with  $Q^2$  has to be explored in depth. Moreover, the role played by the WNC axial-vector form factor is also crucial in understanding the results for the PV asymmetry and its comparison with data. Contrary to some previous works [10, 34–36] where the focus was placed on the analysis of specific data taken at fixed  $|Q^2|$ , here our interest has been to provide a general and coherent description of all data measured at different transferred momenta.

## Acknowledgements

This work was partially supported by DGI (Spain): FIS2008-04189, by the Junta de Andalucía, the Spanish Consolider-Ingenio 2000 programmed CPAN (CSD2007-00042), and part (TWD) by U.S. Department of Energy under cooperative agreement DE-FC02-94ER40818. R.G.J. acknowledges support from the Ministerio de Educación.

## References

- [1] S. Boffi, C. Giusti, F.D. Pacati, *Phys. Rep.* **226** (1993) 1.
- [2] S. Boffi, C. Giusti, F.D. Pacati, M. Radici, *Electromagnetic Response of Atomic Nuclei*, Oxford-Clarendon Press, Oxford (1996).
- [3] J.J. Kelly, *Adv. Nucl. Phys.* **23** Plenum Press, N.Y. (1996).
- [4] J.D. Walecka, *Electron Scattering for Nuclear and Nucleon Structure*, Cambridge University Press, Cambridge (2001).
- [5] A.S. Raskin, T.W. Donnelly, *Ann. Phys.* **191** (1989) 78.
- [6] J. Ashman *et al.*, *Phys. Lett. B [EMC]* **206** (1978) 364.
- [7] V.Y. Alexakhin *et al.* [COMPASS Collaboration], *Phys. Lett. B* **647** (2007) 8.
- [8] A. Airapetian *et al.* [HERMES Collaboration], *Phys. Rev. Lett.* **92** (2004) 012005.
- [9] D.H. Beck, R.D. McKeown, *Annu. Rev. Nucl. Part. Sci.* **51** (2001) 187.
- [10] D. Lhuillier *et al.*, *Prog. Part. Nucl. Phys.* **61** (2008) 183.
- [11] D. von Harrach, *Prog. Part. Nucl. Phys.* **55** (2005) 308.
- [12] J. Gasser, H. Leutwyler, *Phys. Rep.* **87** (1982) 77.
- [13] J.D. Bjorken, S.D. Drell, *Relativistic Quantum Mechanics*, McGraw-Hill, New York (1964).
- [14] T.W. Donnelly, R.D. Peccei, *Phys. Rep.* **50** (1979) 1.
- [15] T.W. Donnelly, J. Dubach, I. Sick, *Phys. Rev. C* **37** (1988) 6.
- [16] M.J. Musolf *et al.*, *Phys. Rep.* **239** (1994) 1.
- [17] J. Liu *et al.*, *Phys. Rev. C* **76** (2007) 025202.
- [18] J. Arrington, I. Sick, *Phys. Rev. C* **76** (2007) 035201.
- [19] J.J. Kelly, *Phys. Rev. C* **70** (2004) 068202.
- [20] E.L. Lomon, *Phys. Rev. C* **66** (2002) 045501.
- [21] E.L. Lomon, *Phys. Rev. C* **64** (2001) 035204.
- [22] C. Crawford *et al.*, *Phys. Rev. C* **82** (2010) 045211.
- [23] M.A. Belushkin, H.-W. Hammer, Ulf-G. Meißner, *Phys. Rev. C* **75** (2007) 035202.
- [24] R. González-Jiménez, J.A. Caballero, T.W. Donnelly, arXiv:1111.6918v1 [nucl-th] 29 Nov 2011, submitted to *Phys. Rep.*
- [25] D. Androić *et al.* [G0 Collaboration], *Phys. Rev. Lett.* **104** (2010) 012001.
- [26] D.T. Spayde *et al.* [SAMPLE Collaboration], *Phys. Rev. Lett.* **84** (2000) 1106.
- [27] S. Baunack *et al.*, [PVA4] *Phys. Rev. Lett.* **102** (2009) 151803.
- [28] K.A. Aniol *et al.* [HAPPEX-99], *Phys. Rev. C* **69** (2004) 065501.
- [29] K.A. Aniol *et al.* [HAPPEX-a], *Phys. Lett. B* **635** (2006) 275.
- [30] A. Acha *et al.* [HAPPEX-b], *Phys. Rev. Lett.* **98** (2007) 032301.
- [31] F.E. Maas *et al.* [PVA4], *Phys. Rev. Lett.* **93** (2004) 022002.
- [32] F.E. Maas *et al.* [PVA4], *Phys. Rev. Lett.* **94** (2005) 152001.
- [33] D.S. Armstrong *et al.* [G0 Collaboration], *Phys. Rev. Lett.* **95** (2005) 092001.
- [34] R.D. Young *et al.*, *Phys. Rev. Lett.* **97** (2006) 102002.
- [35] A.W. Thomas, R.D. Young, *Nucl. Phys. A* **782** (2007) 1.
- [36] A.W. Thomas, R.D. Young, *Nucl. Phys. A* **790** (2007) 173.